Induction of DNA damages upon Marek's disease virus infection: implication in viral replication and pathogenesis

Djihad Bencherit, Sylvie Rémy, Yves Le Vern, Tereza Vychodil, Luca D. Bertzbach, Benedikt B. Kaufer, Caroline Denesvre, Laëtitia Trapp-Fragnet

Induction of DNA damages upon Marek's disease virus infection: implication in viral replication and pathogenesis

Running title: DNA damage upon MDV infection

Djihad Bencherit,[a] Sylvie Remy,[a] Yves Le Vern,[b] Tereza Vychodil,[c] Luca D. Bertzbach,[c] Benedikt B. Kaufer,[c] Caroline Denesvre,[a] and Laëtitia Trapp-Fragnet[a]

[a] *INRA, UMR1282, Infectiologie et Santé Publique, Equipe Biologie des Virus Aviaires, Nouzilly, France*

[b] *INRA, UMR1282 Infectiologie et Santé Publique, Laboratoire de Cytométrie, Nouzilly, France*

[c] *Institut für Virologie, Freie Universitaet Berlin, Berlin, Germany*

Corresponding author: Laëtitia Trapp-Fragnet, INRA, UMR1282, Infectiologie et Santé Publique, Equipe Biologie des Virus Aviaires, Nouzilly, France; Tel: +33 2 474 279 42; email: laetitia.trapp-fragnet@inra.fr

Abstract: 188 words / Importance: 134 words / Text: 5751 words

ABSTRACT

Marek's disease virus (MDV) is a highly contagious alphaherpesvirus that infects chickens and causes a deadly neoplastic disease. We previously demonstrated that MDV infection arrests cells in S-phase and that the tegument protein VP22 plays a major role in this process. In addition, expression of VP22 induces double strand breaks (DSB) in the cellular DNA, suggesting that DNA damage and the associated cellular response might be favorable for the MDV lifecycle. Here, we addressed the role of DNA damage in MDV replication and pathogenesis. We demonstrated that MDV induces DSB during lytic infection *in vitro* and in the PBMCs of infected animals. Intriguingly, we did not observe DNA damage in latently infected MDV-induced lymphoblastoid cells, while MDV reactivation resulted in the onset of DNA lesions, suggesting that DNA damage and/or the resulting DNA damage response might be required for efficient MDV replication and reactivation. In addition, reactivation was significantly enhanced by the induction of DNA damage using a number of chemicals. Finally, we used recombinant viruses to show that VP22 is required for the induction of DNA damage *in vivo* and that this likely contributes to viral oncogenesis.

IMPORTANCE

Marek's Disease Virus is an oncogenic alphaherpesvirus that causes fatal T-cell lymphomas in chickens. MDV causes substantial losses in poultry industry and is also used as a small-animal model for virus-induced tumor formation. DNA damage is not only implicated in tumor development but also aids in the life cycle of several viruses, however its role in MDV replication, latency and reactivation remains elusive. Here, we demonstrated that MDV induces DNA lesions during lytic replication *in vitro* and *in vivo*. DNA damage was not observed in latently infected cells, however is reinitiated during reactivation. Reactivation was significantly enhanced by the induction of DNA damage. Recombinant viruses that lacked the ability to induced DNA damage were defective in the induction of tumors, suggesting that DNA damage might also contribute to cellular transformation processes leading to MDV-lymphomagenesis.

Keywords: Herpesvirus, Marek's disease virus, DNA damage, oncogenesis, viral replication, VP22

INTRODUCTION

Marek's disease (MD) is an oncogenic lymphoproliferative disease caused by the Marek's disease virus (MDV), also referred as to *Gallid herpesvirus 2*. MDV is a member of the *Alphaherpesvirinae* subfamily, mostly due to its genomic organization. However, MDV shows similarities with gammaherpesviruses considering its lymphotropic nature and oncogenic properties (1). Infection of susceptible chickens with very virulent MDV strains induces a rapid onset of tumors within 3-4 weeks and a high mortality. Intriguingly, MDV and the human herpesvirus 6 (HHV-6) integrate their genome into the telomeres of latently infected cells (2-5), allowing the long-life persistence of the virus in the host. Therefore, MDV is used to assess herpesvirus integration as well as virus-induced lymphomagenesis (6). The MDV life cycle is complex and can be broken down into four phases (7, 8): (i) an early cytolytic phase, corresponding to the replication of MDV in B- and T-lymphocytes during the first week of infection; (ii) the establishment of a latent infection in CD4+ T-lymphocytes between 7-10 days post-infection (dpi) during which MDV is thought to integrate its genome into host telomeres ; (iii) the reactivation of the virus from latently infected cells, which is accompanied by its late replication and continuous shedding of the virus from the feather follicle epithelium; and (iv) the tumorigenic phase characterized by transformation of CD4+ T-lymphocytes and the development of T-cell lymphoma.

Several viral oncogenes have been identified such as the latent oncoprotein Meq and the viral telomerase RNA subunit, vTR (9-15), however the exact mechanism leading to lymphoma development remains poorly understood. We recently demonstrated that during lytic replication MDV triggers cell proliferation and subsequently delays the cell cycle in S-phase (16). In addition, we showed that the tegument protein VP22 is able to induce the S-phase arrest in the absence of other viral proteins. This blockade is associated with a massive onset of double strand breaks (DSBs). The VP22 tegument protein is encoded by the UL49 viral

78 gene and is part of the MDV virion. VP22 is involved in cell-to-cell spread of MDV and is
79 essential for MDV replication (17). Beyond its role in MDV replication, VP22 potentially
80 contributes to the establishment of latency and/or transformation by its ability to interact with
81 DNA/histones, to interfere with the cell cycle progression, and to mediate DNA damage.
82 Moreover, it was shown that a recombinant MDV expressing a VP22 with a C-terminal GFP-
83 tag is highly attenuated *in vivo*, suggesting that VP22 plays a role in MDV-induced
84 tumorigenesis (18). In addition, we have previously observed that such a modification of the
85 VP22 C-terminus abolishes its ability to modulate the cell cycle and to induce DNA damage
86 upon overexpression of the protein in proliferating cells (16). Of note, the fusion of GFP to
87 the N-terminus of VP22 did not affect these properties *in vitro* and only mildly attenuates the
88 virus *in vivo* (16, 19).
89 Chromosomal aberrations and modulation of DNA damage response (DDR) are commonly
90 encountered during viral infections and are important for the viral life cycle as reviewed
91 previously (20-26). This has been particularly evidenced in herpesvirus infections for which
92 the ATM (Ataxia Telangiectasia-mutated) and ATR (ATM and Rad3 related) DNA damage
93 pathways proteins play a beneficial role for viral replication (27-31). Effectors of the DDR
94 and DNA repair pathways also facilitate virus maintenance and the establishment of latency
95 (31-33). Moreover, in the case of oncogenic viruses such as the Epstein Barr virus (EBV) and
96 the Kaposi sarcoma-associated herpesvirus (KSHV), the deregulation of these pathways and
97 the induction of DNA damage are of particular importance since genomic instability promotes
98 the establishment of neoplastic processes (34-40). DNA damage has been previously observed
99 in the blood of chickens diagnosed with MD infected with uncharacterized field viral strains
100 (41), however it remained unclear if this damage occurs in lymphocytes and if this is also the
101 case during early infection.

In the present study, we aimed to elucidate the kinetics of DNA damage in MDV infection to determine the role of DNA damage on the MDV life cycle. We demonstrated that DNA breaks accumulate in lytically infected cells *in vivo* and *in vitro*, but not in latently infected cells. We also showed that DNA damage and/or DDR are actively induced upon MDV lytic replication and reactivation from the latent stage. We demonstrated *in vivo* that VP22 is required for the induction of DNA damage using recombinant viruses. Also, we observed that a recombinant virus that lacked the ability to induced DNA damage was defective in the induction of tumors, suggesting that DNA damage induction might participate to the oncogenicity of MDV.

MATERIALS AND METHODS

Cells and viruses

Chicken embryo skin cells were prepared from 12 day-old specific pathogen-free (SPF) White Leghorn (LD1) embryos and maintained in culture as previously described (42). The MDCC-3867K cell line was derived from a renal lymphoma induced upon infection of chicken with the highly pathogenic recombinant vRB-1B 47EGFP virus encoding the UL47 gene fused to the enhanced green fluorescent protein (EGFP) (43). 3867K cells were cultured in RPMI 1640 supplemented with 2 mM glutamine, 1% pyruvate, 1% non-essential amino acids, 1% glucose, 10% tryptose phosphate broth and 10% fetal bovine serum (FBS) and maintained at 41 °C in a 5% CO_2 atmosphere. RECC-CU91 T-cells, a reticuloendotheliosis virus (REV)-transformed chicken T-cell line, were cultured in RPMI 1640 supplemented with 1% pyruvate, 1% non-essential amino acids, 10% fetal bovine serum (FBS) and penicillin/streptomycin, and maintained at 41°C in a 5% CO_2 atmosphere (44).

To visualized virus infected cells, EGFP was fused to the 5' end of the UL49 gene in the avirulent BAC20, resulting in recEGFPVP22 (45). Very virulent, spread competent vRB-1B

127 virus was reconstituted from the infectious bacterial artificial chromosome (BAC) of RB-1B
128 as described previously (46). In addition, recombinant RB-1B were previously generated with
129 EGFP fuses to the 5' and 3' end of VP22, termed vRB-1B EGFP22 and vRB-1B 22EGFP
130 respectively (18, 19). All recombinant viruses were reconstituted, propagated and titrated as
131 described previously (45).

132 Infections of RECC-CU91 T-cells were performed by co-cultivation with infected CESCs
133 (47). One million CESCs were infected with 3 x 10^4 PFU of RB-1B_TK-GFP that expresses
134 GFP under the control of the early HSV-1 TK promoter for 3-4 days in 6-well plates.
135 Subsequently, 10^6 RECC-CU91 T-cells were added to the highly infected CESCs monolayer
136 for 16 hours at 41°C. RECC-CU91 cells were carefully removed at day 1, 2 and 3 post-
137 infection for further analysis.

138 **Pharmacological induction of DNA damages**

139 DNA damage was induced in cells by etoposide (ETP; Sigma-Aldrich), bleomycin
140 (Calbiochem), hydroxyurea (HU; Sigma-Aldrich) and hydrogen peroxide (H_2O_2; Sigma-
141 Aldrich) treatments. At 6h post-infection, CESCs infected with the recEGFPVP22 were
142 treated by addition in the culture media of the pharmacological agents at appropriate
143 concentrations (0.033, 0.066 or 0.132 µM of ETP; 0.125 to 1 µM of bleomycin; 10 to 75 µM
144 of HU and 12.5 to 100 µM of H_2O_2). ETP treated infected cells were analyzed at 24, 48, 72,
145 and 96h post-infection and bleomycin, hydroxyurea and hydrogen peroxide treated cells at
146 72h. RECC-CU91 cells were treated at the time of infection with 0.02 µM or 0.1 µM ETP for
147 24, 48 and 72h pi. Treatments of 3867K cells were performed for 48h with 0.004 to 0.5 µM of
148 ETP; 1 to 25 µM of bleomycin; 0.0625 to 1 mM of HU and 0.1 to 1 mM of H_2O_2. In all
149 experiments, DMSO (for ETP) or H_2O (for bleomycin, HU and H_2O_2) was used as negative
150 control and added in the culture medium at a volume equivalent to the corresponding to the
151 highest concentration of drug treatments.

Animal experiments

Two *in vivo* experiments were conducted in this study according to the guidelines and regulations as outlined that were approved by the local ethic committee "Comité d'Ethique pour l'Expérimentation Animale de Val de Loire" (CEEA VdL, protocol number 2012-09-3). In the first experiment (Fig. 4), 24 days-old SPF white leghorn chicks (B13/B13 haplotype) were infected intramuscularly (pectoral muscles) with 1,000 pfu of vRB-1B (n=13) or mock infected (n=10) and housed in isolation units. In the second experiment (Fig. 5), chickens were either infected with 1,500 pfu of vRB-1B (n=6), vRB-1B EGFP22 (n=12), vRB-1B 22EGFP (n=13) or mock infected (n=10) as described above. Of note, in order to inoculate an equal amount of virus to chickens, vRB-1B EGFP22 and vRB-1B 22EGFP viral inoculum were exclusively constituted of EGFP+ positive sorted CESCs (i.e. infected cells). Birds were evaluated daily for symptoms of MD. In the case of clinical evidence of MD, the chickens were euthanized and examined postmortem for the presence of gross MD lesions. At the end of the experiments (35 dpi in experiment #1 and 49 dpi in experiment #2), all surviving birds were euthanized and necropsied. To assess the DNA damage in peripheral blood mononuclear cells and to follow the viral load, blood was collected on 3% sodium citrate from all birds at 0, 7, 14, 21, 28 and 35 dpi for experiment #1 and 0, 7, 14, 21, 28, 35 42 and 49 dpi for experiment #2. PBMCs were isolated from 1 ml of whole blood using lymphocytes-separation medium LSM (Eurobio, France) as previously described (19).

DNA extraction and real-time quantitative PCR (qPCR)

To quantify the viral load, DNAs were extracted from 30 µl whole blood (animal experiment #1) or from $2x10^6$ isolated cells (PBMCs in the animal experiment #2, CESC and RECC-CU91 cells), using the QIAamp DNA mini kit according to the manufacturer's instructions (Qiagen). MDV genome copies were quantified by qPCR as previously described (19, 48).

176 The MDV genome was detected using primers and probes against the ICP4 gene and was
177 normalized to 10^6 copies of cellular genome quantified by the detection of the iNOS gene.

178 **RNA extraction and quantitative Reverse Transcription-PCR (qRT-PCR)**

179 RNAs were extracted from 10^6 non-infected and recEGFPVP22 infected CESCs, PBMCs
180 isolated from vRB-1B infected chickens and 3867K cells, using the RNeasy Mini kit
181 following the manufacturer's instructions (Qiagen). RNAs were treated with RNAse-free
182 RQ1 DNAse (Promega, France) and the RNA concentration was measured with a NanoDrop
183 spectrophotometer. One µg of total RNA was reverse transcribed using 100 µg/mL oligo(dT)
184 primers (Promega) and M-MLV reverse transcriptase (Promega). The expression of the genes
185 of interest was then assessed by qRT-PCR using the Supermix SYBR green (Bio-Rad) as
186 previously described (16). The sequence of the specific primer pairs used for the amplification
187 of the viral and cellular genes are depicted in Table 1. Expression of the chicken
188 glyceraldehyde phosphate dehydrogenase (GAPDH) was used for the normalization and the
189 relative changes in gene expression were determined by the 2(-ΔΔCT) method.

190 **Cell sorting and flow cytometry analysis**

191 Sorting of CESCs infected with recombinant viruses expressing fluorescent VP22 proteins
192 were performed at 4 dpi. The 3867K cells exhibiting MDV lytic replication were sorted on the
193 basis of the expression of the UL47 protein tagged with EGFP. Mock-infected CESCs
194 (negative control) were also sorted to avoid experimental bias linked to sorting. Damaged
195 cells and debris were eliminated on the basis of morphological criteria. EGFP positive and
196 negative cells were sorted using a MoFlo® high-speed cell sorter (Beckman Coulter, Fort
197 Collins, CO, USA).
198 The percentage of lytically infected 3867K and RECC-CU91 T cells was determined by
199 cytometry on the basis of the expression of the GFP (associated to the expression of UL47
200 and TK-promoter, respectively). Cell viability was estimated using the fixable viability dye

eFluor® 780 (eBioscience) at dilution of 1:1000. Staining was performed for 15 minutes on ice in the dark. Cells were washed twice in PBS before being fixed with paraformaldehyde (PAF) 1%. Cell viability was analyzed with a 780/40 nm band-pass filter.

Alkaline comet assay

Alkaline comet assays were performed from $2x10^5$ cells as previously described (16, 49). Two slides for comet assays were prepared for each condition. Comets were observed using the Axiovert 200 M inverted epifluorescence microscope (Zeiss) and images were taken with an Axiocam MRm camera (Zeiss). A minimum of 50 comets was analyzed for each replicate using the CometScore software version 1.5 (TriTek). The olive tail moment parameter (OTM) was calculated on the basis of the tail length and the relative proportion of DNA contained in the tail. Results are presented as the mean (±SD) of the OTM calculated for each condition or as a distribution of the comets with respect to their respective OTM value (i.e. the percentage of cells presenting a defined OTM).

Reactive oxygen species (ROS) assay

ROS production was assayed from supernatant (80µl) of mock- and recEGFPVP22-infected CESCs at 24h, 48h, 72h and 96h pi using the ROS-Glo™ H_2O_2 assay following manufacturer's instructions (Promega). Luminescence quantification was performed using a Glomax® Multidetection system luminometer (Promega). Results were recorded as relative luminescent units (RLU). Assays were done in triplicates at each time point. Results obtained from infected-cells were normalized to that of mock-infected conditions and expressed as means (±SD).

Nitric oxide (NO) assay

NO produced from infected and mock-infected CESCs was measured at 24, 48, 72 and 96 hpi by detecting the accumulation of nitrite (NO_2^-) in the culture media using the Griess reaction (50). Fifty microliters of cell culture supernatant were collected at each time point in a 96-

well plate (in triplicates) and incubated for 10 min in the dark with 100 µl of Griess reagent (mixture (1:1) of 1% sulfanilamide (Sigma-Aldrich) in 1.2 N hydrochloric acid and 0.3% N-1-naphthylethylenediamine dihydrochloride (Sigma-Aldrich)). Absorbance was then measured at 540 nm. Nitrite concentrations were calculated with reference to a calibration curve established using standard solutions ranging from 0 to 200 µM of sodium nitrite (Sigma-Aldrich) diluted in culture medium. A positive control consisting of supernatant of *E.coli* infected cells was included in the assay as well as cell-free media as negative control.

Fluorescence Microscopy

CESCs were grown on glass coverslips and infected with recEGFPVP22. At 4 days pi, infected and non-infected cells were fixed with 4% PFA for 20 min at room temperature (RT) and permeabilized with 0.5% Triton X-100 for 5 min at RT. After blocking with PBS, 0.1% Triton X-100 and 2% Bovine Serum Albumin (BSA), cells were incubated with mouse monoclonal IgG directed against phospho-histone H2AX (Ser139) (Millipore; clone JBW301) at a dilution of 1:500. Goat anti-mouse IgG Alexa-Fluor 594 secondary antibody (Invitrogen) was used at 1:2000. Nuclei were counterstained with Hoechst 33342 (Invitrogen). EGFP fluorescence was directly observed from cells expressing the viral EGFP-tagged VP22 protein. Cells were observed under an Axiovert 200 M inverted epifluorescence microscope equipped with a 40× PlanNeofluar oil/Dic objective or a 63× PlanApochromat oil/DIC and the Apotome imaging system (Zeiss). Images were captured with a CCD Axiocam MRm camera (Zeiss) by using the Axiovision software.

MDV plaque size measurement assay

At 48 hpi, CESCs monolayers infected with the recEGFPVP22 virus and treated with ETP were fixed with 4% PFA. Fluorescence emitted from the viral EGFP-tagged VP22 protein was detected using Axiovert 200 M inverted epifluorescence microscope equipped with a 5× Fluar objective. Viral plaques were measured and analyzed as previously described (45).

Statistical analysis

All graphs and statistics were performed using the GraphPad Prism software version 5.02 (San Diego, USA). Data are presented as means and standard deviations (±SD) or medians. The one-way ANOVA test was used to compare differences in multiple groups and the Mann-Whitney (two-tailed) was used to compare nonparametric variables between two groups. Significant differences were determined using Student's *t*-test. *P* values <0.05 were considered statistically significant as indicated in the figure legends.

RESULTS

MDV replication induces double strand breaks in the host genome

Until now, it remained unknown if MDV induces DNA damage during virus replication. Therefore, we infected CESCs with a recombinant virus containing EGFP fused to the N-terminus of VP22 (recEGFPVP22). GFP-positive MDV infected and GFP-negative cells were sorted by flow cytometry 96 hpi and DNA damage was assessed by alkaline comet assay. MDV infection increased the rate of DNA damage by 8.5-fold and 6-fold compared to GFP-negative and mock-infected cells, respectively (Fig. 1A). In addition, up to 30% of the infected cells had an OTM score greater than 10, indicative of highly damaged DNA (Fig. 1B). To identify the nature of the DNA damage in infected cells, we monitored the expression and localization of γ-H2AX, a marker classically used to detect double strand breaks (DSBs). Immunofluorescence analyses revealed a significant increase in intensity of γ-H2AX and a typical localization of the protein as foci in the nucleus of CESCs infected with the recEGFPVP22 virus (Fig. 1C) indicative of the presence of DSBs.

Induction of DNA damage enhances MDV replication

To determine if the induction of DNA damage and/or the subsequent DDR is beneficial for MDV replication, we infected CESCs with recEGFPVP22 in the presence or absence of potent DSB inducer etoposide (ETP) (51) and monitored MDV replication by qPCR (Fig. 2A

and B). MDV replication was significantly increased in the presence of ETP at 96 hpi compared to DMSO treated control cells, and the greatest increase was observed for the highest ETP concentration (Fig. 2A and B). To confirm that the observed effect is indeed due to the induction of DNA damage, we also tested a number of pharmacological agents known to generate single-strand and DSB, replicative stress and/or oxidative stress (bleomycin, hydroxyurea (HU) and H_2O_2). As for ETP treatment, CESCs were infected with recEGFPVP22 and treated with these drugs at different concentrations and MDV copy number was assayed at by qPCR (Table 2). The overall effect of the DNA damaging agents tested was more moderate than ETP on MDV infected-cells, although all reagents tended to increase slightly viral replication, underlining that DNA damage enhances MDV replication. In addition, we could demonstrate that ETP increases the percentage of viable GFP-VP22 expressing cells in a dose dependent manner when compared to DMSO-treated control cells (Fig. 2C). This increase in infected cells was significant for the highest ETP concentrations. Furthermore, MDV plaques were also significantly larger upon induction of DNA damage (Fig. 2D), indicating that the virus spread more efficiently to surrounding cells. Beyond that, we also assessed the effect of ETP treatment on MDV replication in T cells, the natural target of MDV infection. RECC-CU91 T cell were infected with RB-1B_TK-GFP in presence of ETP and MDV copy number was monitored by qPCR (Fig. 2E). The impact of ETP treatment on MDV replication in T-cells is more mitigated than in CESCs, however MDV genome copies slightly increase from one day pi when cells were treated with the highest ETP concentration.

Taken together, our data demonstrate that additional induction of DNA damage and/or the subsequent DDRs are beneficial for MDV replication.

MDV replication induces reactive oxygen species (ROS) and nitric oxide (NO) production in CESCs

Next we assessed if MDV induced DNA damage is mediated by oxidative stress, a common cause of DSBs (52). We first monitored the level of ROS by measuring the production of hydrogen peroxide (H_2O_2) in the supernatant of MDV or mock-infected cells (Fig. 3A). A significant accumulation of H_2O_2 was detected in the supernatant of infected cells from 48 to 96 hpi. Besides ROS, reactive nitrogen species such as nitric oxide (NO) also plays a role in metabolic stress and oxidative DNA damage in cells (53). We measured NO production in the supernatant of infected and mock-infected cells and observed a significant increase of NO at 72 hpi (Fig. 3B). NO can be generated by the inducible nitric oxide synthases (iNOS) that is generally activated upon immune response. Intriguingly, NO production coincided with an increase expression of iNOS at 72 hpi (Fig. 3C). Our data suggest that MDV infection is associated with an increased level of reactive oxygen and nitrogen species that could contribute to the DNA damage in infected cells.

DNA damage induction in chicken peripheral blood mononuclear cells upon MDV infection

To determine if MDV induces DNA lesions *in vivo*, we infected chickens with the very virulent MDV strain vRB-1B. Blood was collected from all animals at various time points. Viral load was assessed by qPCR on whole blood and DNA damage was determined using the alkaline comet assay on isolated peripheral blood mononuclear cells (PBMCs). In addition, the establishment of viral latency was followed by analyzing the mRNA expression of Meq by qRT -PCR in non-infected and vRB-1B infected PBMCs. Intriguingly, DNA damage was significantly increased (about 3-fold higher) in PBMCs of infected chickens during the lytic phase of the MDV life cycle at 7 dpi (Fig. 4A). In contrast, no increase in DNA lesions was observed in the latent phase of infection after 14 dpi. The increased in DNA damage was

326 associated with a 100-fold increase in viral load in the blood during the lytic phase of
327 infection (Fig. 4B). After day 14, high levels of the major oncogene Meq were observed by
328 qRT-PCR, corresponding to latently infected or MDV transformed cells (Fig. 4C) and are in
329 agreement with previous reports on the establishment of latency (54, 55). Thus, our data
330 shows that MDV early lytic infection is associated with transient DNA damage in PBMCs,
331 while no DNA damage was detected at later stages of infection.

332 **VP22 contributes to the DNA damage upon MDV infection *in vivo*.**

333 We previously demonstrated that overexpression of VP22 arrests the cell cycle and induces
334 DNA damage *in vitro* (16). In addition, we showed that MDV harboring EGFP fused to the C-
335 terminus of VP22 (vRB-1B 22EGFP) is severely attenuated, while fusion to the N-terminus of
336 VP22 (vRB-1B EGFP22) induces only a mild decrease in oncogenicity (18, 19), suggesting
337 that the C-terminal fusion affects VP22 function. Based on this observation, we assess the
338 induction of DNA damage mediated by these recombinant viruses *in vivo.* We infected SPF
339 chickens with either wild-type vRB-1B, vRB-1B 22EGFP or vRB-1B EGFP22 and monitored
340 DNA damage, virus replication and tumor development. Intriguingly, DNA damage at day 7
341 was only observed in PBMCs of birds infected with wild-type vRB-1B and vRB-1B EGFP22,
342 suggesting that the fusion of GFP to the N terminus of VP22 does not affect DNA damage
343 induction (Fig. 5A). In contrast, levels of DNA damage in PBMCs of vRB-1B 22EGFP
344 infected animal was comparable to mock infected chickens, indicating that fusion of GFP to
345 the C-terminus of VP22 disrupts its ability to mediate DNA lesions. To ensure that this effect
346 was not just due to a reduced virus replication, we monitored virus load in PBMCs by qPCR
347 and could demonstrate that virus replication was only mildly reduced at day 7. In contrast, a
348 significant decrease was observed at days 14 and 28 pi between vRB-1B 22EGFP and the
349 parental virus (Fig. 5B). Since DNA damage also plays an important role in cancer
350 development, we also monitored tumor incidence in the infected chickens. As observed

351 previously, tumor formation was severely impaired for vRB-1B 22EGFP (31 %) that cannot
352 induce DNA damage, while tumors were efficiently induced by wild-type vRB-1B (100 %)
353 and vRB-1B EGFP22 (66%). Our data shows that DNA damages is dependent on a functional
354 VP22 and that tumor formation is severely impaired for a virus that cannot induce DNA
355 damage.

356 **MDV reactivation is accompanied and enhanced by DNA damage**

357 Next, we set to determine if DNA damage is induced upon MDV reactivation. We
358 used a lymphoblastoid cell line that expresses GFP fused to the tegument protein UL47 upon
359 reactivation (3867K) as described previously (43). We sorted EGFP positive and negative
360 cells and assessed DNA damage by comet assays. DNA damage was significantly increased
361 in reactivating (GFP+) cells compared to the latent, GFP negative cells (Fig. 6A), indicating
362 that MDV reactivation in T cells is associated with DNA damage. An increased proportion of
363 reactivating cells also showed high levels of DNA damage (8%, OTM>10), while only
364 minimal damage is seen in latently infected cells (Fig. 6B). Next, we evaluated if DNA
365 damage can also increase reactivation. We induced DNA damage in 3867K with increasing
366 concentration of ETP for 48 hours. Both ICP4 expression and the number of GFP expressing
367 cells was significantly increased in a dose dependent manner (Fig. 6C and D). To confirm that
368 effect of DNA damage on MDV reactivation, we treated 3867K cells with bleomycin, HU and
369 H_2O_2. MDV reactivation was significantly increased in a dose dependent manner for all three
370 DNA damage inducing drugs (Fig. 6E). Taken together, our data demonstrate that DNA
371 damage is induced upon MDV reactivation and that induction of DNA damages seem to be
372 favorable for MDV reactivation.

373 **DISCUSSION**

374 The hallmark of the present study is the observation of an onset of DNA lesions in cells
375 sustaining MDV replication *in vitro* and *in vivo*. This was initially shown *in vitro* in MDV-

376 infected CESCs in which we detected DNA DSBs at 96 hpi. *In vivo*, we demonstrated that
377 MDV early cytolytic replication is associated with an increase in DNA damages in PBMCs of
378 infected chickens early after infection (7 dpi). Moreover, we showed *in vitro* that
379 lymphoblastoid cells (3867K) undergoing MDV replication induced from the spontaneous
380 reactivation of the virus are also affected by DNA damage. Of note, DNA damage during
381 MDV reactivation in the PBMCs of birds infected with the highly virulent RB-1B was not
382 statistically significant different from that of the mock-infected birds at 21 dpi, the time point
383 at which a peak of viral reactivation is expected. This might be due to the fact that only a
384 small number of CD4+ T cells reactivate in the blood and the low sensitivity of the comet
385 assay.

386 Intriguingly, DNA lesions were detected at 7 dpi in the PBMCs of chickens infected with both
387 vRB-1B or vRB-1B EGFP22 virus, but not with the attenuated vRB-1B 22EGFP virus, even
388 though all 3 viruses showed similar robust viral DNA replication as was assessed by qPCR
389 results. This observation may indicate that MDV replication is not sufficient to induce DNA
390 breaks. However, at 14 and 28 dpi the attenuated vRB-1B 22EGFP virus displayed a lower
391 replication rate compared to the wild-type vRB-1B virus. We could assume that this growth
392 defects might be associated with the low rate of DNA lesions occurring during the early
393 replication of the virus (at 7 dpi), and thus that DNA damage might be favorable for MDV
394 replication. These observations also confirmed that VP22 is a major viral determinant
395 associated to DNA damages *in vivo*. The VP22 tegument protein is abundantly expressed
396 during viral lytic infection and essential for MDV replication (17, 42). In a previous study, we
397 also reported that the overexpression of VP22 leads to DSB induction in proliferating cells,
398 and that this activity of VP22 depends on an unmodified C-terminal extremity (16). Herein,
399 we show *in vivo*, in an infectious context, that VP22 is involved in the induction of DNA
400 lesions observed during MDV early cytolytic infection, and that the modification of the C-

terminal extremity of the protein subverted the ability of MDV to trigger DNA damage in PBMCs. It should also be noted that the level of DNA lesions detected at 7 dpi in PBMCs from infected birds is somewhat surprising given the low number of circulating infected cells and seems to indicate that non-infected cells might also be subjected to DNA damage. The lesions observed in the non-infected population could be attributed to the inflammatory immune response and/or paracrine signaling molecules emitted from infected cells and responsible of a bystander effect (56-58). Also, despite conflicting reports about the intercellular trafficking property of the VP22 protein, we cannot exclude that VP22 could spread to non-infected surrounding cells and contribute to the generation of DNA lesions in these cells (59-61). The mechanism by which VP22 is involved in the onset of DNA lesions is still unclear. MDV VP22 could have a direct genotoxic activity on DNA since VP22 can interact with DNA and histones (16, 42), or could activate cellular metabolism pathways leading to DNA damage. In support to the latter hypothesis, we showed that MDV infection triggers oxidative stress in CESC. We detected an increase of hydrogen peroxide production from 48 hpi in CESCs infected with MDV. In addition, a higher level of nitrites associated to an increase of iNOS mRNA expression was detected at 72 hpi in the supernatant of MDV-infected CESCs compared to mock-infected cells. Previous studies reported that MDV infection influences the production of NO (41, 48). A correlation was notably established between the virulence of MDV strains and its ability to induce NO, with the most virulent strains inducing the highest level of NO (48). It is believed that NO plays a role in MDV pathogenesis through its involvement in the immune suppression observed early after infection (48). Nevertheless, the role of NO on MDV replication is still not clearly elucidated. NO production was identified as an anti-viral process by inhibiting MDV replication *in vitro* and *in vivo* (62, 63). However, Jarosinski *et al*. demonstrated that despite a high NO response, chickens infected with very virulent MDV strains showed an enhanced cytolytic infection

(48). Oxidative stress is a major generator of DNA breaks including DSBs (64). We could thus hypothesize that oxidative stress generated during MDV replication could participate in the generation of DNA lesions, which in turn would facilitate MDV replication and consequently potentiate the virulence of MDV. We have indeed demonstrated that DNA damage seems to favor the replication of the virus, since we have shown that DNA damaging pharmacological agents can promote MDV replication and enhance MDV reactivation from latent infection. Of note, the impact on MDV replication seemed to depend on the drug used and thus probably on the nature of the damages generated and/or the damage response (DDR) associated. Also, the response to different treatments might vary between cells according to their lineage (lymphoid, fibroblastic) and their proliferative potential (primary versus cell lines). Hence, ETP treatment (inducing mainly DSBs) resulted in an increase of MDV replication in CESCs, while bleomycin, hydroxyurea and H_2O_2 treatments had a weaker effect in CESCs. One explanation might be the low proliferative rate of CESCs that may counteract the activity of drugs inducing damage during S phase. ETP had also mild effect on MDV replication in CU-91 T- cell line. Also, CU-91 were initially transformed with REV, we could thus hypothesize that the presence of a replicative retrovirus might disturb the DNA damage responses in these cells and/or have an impact on MDV replication. On the other hand, all treatments induced a significant increase of MDV reactivation in a lymphoid cell line transformed by MDV. We cannot currently specify whether DNA damages only or the induction of the DDR associated with the onset of damage promotes MDV replication. As previously demonstrated for a number of viruses and especially herpesviruses, the DNA damage response (DDR) plays a major role in viral replication (for review see (20, 22-24, 26, 65)). Unfortunately, we were not able to characterize more precisely the DDR pathways induced during MDV infection in the present study due to a lack of specific tools cross-reacting with chicken proteins. Nevertheless, we hypothesized that MDV infection induces

451 the activation of a DDR as it was demonstrated for other herpesviruses. We identified at least
452 two processes that could contribute to the DDR pathways activation: (i) the generation of
453 DNA lesions in cellular DNA triggered upon MDV replication, and (ii) the increase of
454 oxidative stress in MDV-infected CESCs. Elevated levels of ROS are known to activate DDR
455 pathways, as demonstrated notably upon EBV infection in which the latent protein EBNA1
456 promotes ROS accumulation and consequently ATM-dependent DDR activation (34).
457 Moreover, our previous study demonstrated that MDV induces an S-phase arrest in fibroblasts
458 (16). This constitutive S-phase induction may generate a favorable environment for viral
459 replication but could also lead to replicative stress, a potent mechanism responsible of DDR
460 induction. Although we currently cannot determine the DDR pathways activated by MDV, we
461 can speculate that ATM signaling may be induced in response to the DSBs and to the
462 oxidative stress generated during MDV infection (66, 67). Of note, ATM pathway activation
463 seems to be a common characteristics of herpesviruses infections (as previously reported
464 notably for the human herpesvirus type-1 (HSV-1), the cytomegalovirus (CMV, EBV and
465 KSHV), and in most cases ATM has been demonstrated to be beneficial for viral replication
466 (28, 68-70).

467 Finally, a major point of interest of the present study is the potential involvement of the onset
468 of DNA lesions in MDV-induced lymphomagenesis. Many reports have shown that DNA
469 damage and the DDR can contribute to genomic instability in cells and in turn to the
470 development of tumors. Moreover, DSBs are among the most deleterious lesions occurring in
471 cells and if not repaired, accumulation of DSBs could promote cell-death or the loss of
472 genome integrity possibly leading to carcinogenesis (71). Several studies demonstrated the
473 interplay between oncogenic viruses and DNA damage/DDR signaling and its crucial
474 implication in virus mediated-tumorigenesis (for review see (35, 39, 40)). Our data support
475 these findings since we observed a greater rate of DNA damage in PBMCs from chickens

476 infected with virulent MDV viruses (vRB-1B and vRB-1B EGFP22) and to a significantly
477 lesser extend in PBMCs of birds infected with an attenuated recombinant virus (vRB-1B
478 22EGFP). The low oncogenicity of the vRB-1B 22EGFP virus might well be associated with
479 its diminished replication capacity (as observed at day 14 pi). However, in the light of our
480 results, one can also speculate that the viral phenotype is due to the absence of an early onset
481 of DNA lesions in infected leukocytes that otherwise might contribute to MDV induced
482 tumorigenesis. One hypothesis would be that the enhanced MDV replication upon, could
483 result in an increased number of latently infected cells from which transformed T cells
484 originate. DNA damage could also play a direct role in the establishment of viral latency and
485 more precisely in the integration process of the viral genome. We indeed cannot exclude that
486 the DNA lesions observed at an early time point of MDV infection could arise before or
487 concomitantly to MDV latent infection in CD4+ T-lymphocytes and thus could facilitate
488 MDV genome integration either directly or indirectly by triggering DDR and DNA repair
489 pathways, especially homologous recombination, as it was previously suggested for the
490 hepatitis B virus, human Papillomaviruses, Merkel Cell Polyomavirus and EBV (2, 3, 72, 73).
491 However, one should not underestimate the impact of a potential genomic instability
492 originating from DNA damage generated during MDV replication. It is indeed conceivable
493 that, in a particular sequence of events including cell cycle deregulation, reprogramming of
494 gene expression by viral oncogenes (notably Meq) and telomerase activation, the
495 accumulation of DNA lesions upon MDV infection may also contribute to the transformation
496 process ultimately leading to MD lymphoma formation.

497 **AKNOWLEDGEMENTS**

498 We thank F. Paillard for editing the manuscript, D. Pasdeloup and S. Trapp for their
499 constructive comments and corrections on the manuscript, as well as C. Berthault and K.
500 Courvoisier for their technical help.

REFERENCES

1. **Jha HC, Banerjee S, Robertson ES.** 2016. The Role of Gammaherpesviruses in Cancer Pathogenesis. Pathogens **5**.
2. **Delecluse HJ, Hammerschmidt W.** 1993. Status of Marek's disease virus in established lymphoma cell lines: herpesvirus integration is common. J Virol **67:**82-92.
3. **Kaufer BB, Jarosinski KW, Osterrieder N.** 2011. Herpesvirus telomeric repeats facilitate genomic integration into host telomeres and mobilization of viral DNA during reactivation. J Exp Med **208:**605-615.
4. **Arbuckle JH, Medveczky MM, Luka J, Hadley SH, Luegmayr A, Ablashi D, Lund TC, Tolar J, De Meirleir K, Montoya JG, Komaroff AL, Ambros PF, Medveczky PG.** 2010. The latent human herpesvirus-6A genome specifically integrates in telomeres of human chromosomes in vivo and in vitro. Proceedings of the National Academy of Sciences of the United States of America **107:**5563-5568.
5. **Wallaschek N, Sanyal A, Pirzer F, Gravel A, Mori Y, Flamand L, Kaufer BB.** 2016. The Telomeric Repeats of Human Herpesvirus 6A (HHV-6A) Are Required for Efficient Virus Integration. PLoS Pathog **12:**e1005666.
6. **Osterrieder N, Kamil JP, Schumacher D, Tischer BK, Trapp S.** 2006. Marek's disease virus: from miasma to model. Nat Rev Microbiol **4:**283-294.
7. **Calnek BW.** 2001. Pathogenesis of Marek's disease virus infection. Curr Top Microbiol Immunol **255:**25-55.
8. **McPherson MC, Delany ME.** 2016. Virus and host genomic, molecular, and cellular interactions during Marek's disease pathogenesis and oncogenesis. Poult Sci **95:**412-429.
9. **Burnside J, Bernberg E, Anderson A, Lu C, Meyers BC, Green PJ, Jain N, Isaacs G, Morgan RW.** 2006. Marek's disease virus encodes MicroRNAs that map to meq and the latency-associated transcript. J Virol **80:**8778-8786.
10. **Engel AT, Selvaraj RK, Kamil JP, Osterrieder N, Kaufer BB.** 2012. Marek's disease viral interleukin-8 promotes lymphoma formation through targeted recruitment of B cells and CD4+ CD25+ T cells. J Virol **86:**8536-8545.
11. **Nair V.** 2013. Latency and tumorigenesis in Marek's disease. Avian Dis **57:**360-365.
12. **Trapp S, Parcells MS, Kamil JP, Schumacher D, Tischer BK, Kumar PM, Nair VK, Osterrieder N.** 2006. A virus-encoded telomerase RNA promotes malignant T cell lymphomagenesis. J Exp Med **203:**1307-1317.
13. **Kung HJ, Xia L, Brunovskis P, Li D, Liu JL, Lee LF.** 2001. Meq: an MDV-specific bZIP transactivator with transforming properties. Curr Top Microbiol Immunol **255:**245-260.
14. **Lupiani B, Lee LF, Cui X, Gimeno I, Anderson A, Morgan RW, Silva RF, Witter RL, Kung HJ, Reddy SM.** 2004. Marek's disease virus-encoded Meq gene is involved in transformation of lymphocytes but is dispensable for replication. Proc Natl Acad Sci U S A **101:**11815-11820.
15. **Gimeno IM, Witter RL, Hunt HD, Reddy SM, Lee LF, Silva RF.** 2005. The pp38 gene of Marek's disease virus (MDV) is necessary for cytolytic infection of B cells and maintenance of the transformed state but not for cytolytic infection of the feather follicle epithelium and horizontal spread of MDV. J Virol **79:**4545-4549.
16. **Trapp-Fragnet L, Bencherit D, Chabanne-Vautherot D, Le Vern Y, Remy S, Boutet-Robinet E, Mirey G, Vautherot JF, Denesvre C.** 2014. Cell cycle modulation by Marek's disease virus: the tegument protein VP22 triggers S-phase arrest and DNA damage in proliferating cells. PLoS One **9:**e100004.
17. **Dorange F, Tischer BK, Vautherot JF, Osterrieder N.** 2002. Characterization of Marek's disease virus serotype 1 (MDV-1) deletion mutants that lack UL46 to UL49 genes: MDV-1 UL49, encoding VP22, is indispensable for virus growth. J Virol **76:**1959-1970.

18. **Jarosinski KW, Arndt S, Kaufer BB, Osterrieder N.** 2011. Fluorescently tagged pUL47 of Marek's disease virus reveals differential tissue expression of the tegument protein in vivo. J Virol **86:**2428-2436.
19. **Remy S, Blondeau C, Le Vern Y, Lemesle M, Vautherot JF, Denesvre C.** 2013. Fluorescent tagging of VP22 in N-terminus reveals that VP22 favors Marek's disease virus (MDV) virulence in chickens and allows morphogenesis study in MD tumor cells. Vet Res **44:**125.
20. **Smith S, Weller SK.** 2015. HSV-I and the cellular DNA damage response. Future Virol **10:**383-397.
21. **Fortunato EA, Spector DH.** 2003. Viral induction of site-specific chromosome damage. Rev Med Virol **13:**21-37.
22. **Lilley CE, Schwartz RA, Weitzman MD.** 2007. Using or abusing: viruses and the cellular DNA damage response. Trends Microbiol **15:**119-126.
23. **Sinclair A, Yarranton S, Schelcher C.** 2006. DNA-damage response pathways triggered by viral replication. Expert Rev Mol Med **8:**1-11.
24. **Turnell AS, Grand RJ.** 2012. DNA viruses and the cellular DNA-damage response. J Gen Virol **93:**2076-2097.
25. **Weitzman MD, Carson CT, Schwartz RA, Lilley CE.** 2004. Interactions of viruses with the cellular DNA repair machinery. DNA Repair (Amst) **3:**1165-1173.
26. **Xiaofei E, Kowalik TF.** 2014. The DNA damage response induced by infection with human cytomegalovirus and other viruses. Viruses **6:**2155-2185.
27. **Hau PM, Deng W, Jia L, Yang J, Tsurumi T, Chiang AK, Huen MS, Tsao SW.** 2015. Role of ATM in the Formation of the Replication Compartment during Lytic Replication of Epstein-Barr Virus in Nasopharyngeal Epithelial Cells. J Virol **89:**652-668.
28. **Hollingworth R, Skalka GL, Stewart GS, Hislop AD, Blackbourn DJ, Grand RJ.** 2015. Activation of DNA Damage Response Pathways during Lytic Replication of KSHV. Viruses **7:**2908-2927.
29. **Mohni KN, Dee AR, Smith S, Schumacher AJ, Weller SK.** 2013. Efficient herpes simplex virus 1 replication requires cellular ATR pathway proteins. J Virol **87:**531-542.
30. **Mounce BC, Tsan FC, Droit L, Kohler S, Reitsma JM, Cirillo LA, Tarakanova VL.** 2011. Gammaherpesvirus gene expression and DNA synthesis are facilitated by viral protein kinase and histone variant H2AX. Virology **420:**73-81.
31. **Lilley CE, Carson CT, Muotri AR, Gage FH, Weitzman MD.** 2005. DNA repair proteins affect the lifecycle of herpes simplex virus 1. Proc Natl Acad Sci U S A **102:**5844-5849.
32. **Jha HC, Upadhyay SK, M AJP, Lu J, Cai Q, Saha A, Robertson ES.** 2013. H2AX phosphorylation is important for LANA-mediated Kaposi's sarcoma-associated herpesvirus episome persistence. J Virol **87:**5255-5269.
33. **Tarakanova VL, Stanitsa E, Leonardo SM, Bigley TM, Gauld SB.** 2010. Conserved gammaherpesvirus kinase and histone variant H2AX facilitate gammaherpesvirus latency in vivo. Virology **405:**50-61.
34. **Gruhne B, Sompallae R, Masucci MG.** 2009. Three Epstein-Barr virus latency proteins independently promote genomic instability by inducing DNA damage, inhibiting DNA repair and inactivating cell cycle checkpoints. Oncogene **28:**3997-4008.
35. **Hollingworth R, Grand RJ.** 2015. Modulation of DNA damage and repair pathways by human tumour viruses. Viruses **7:**2542-2591.
36. **Koopal S, Furuhjelm JH, Jarviluoma A, Jaamaa S, Pyakurel P, Pussinen C, Wirzenius M, Biberfeld P, Alitalo K, Laiho M, Ojala PM.** 2007. Viral oncogene-induced DNA damage response is activated in Kaposi sarcoma tumorigenesis. PLoS Pathog **3:**1348-1360.
37. **Wu CC, Liu MT, Chang YT, Fang CY, Chou SP, Liao HW, Kuo KL, Hsu SL, Chen YR, Wang PW, Chen YL, Chuang HY, Lee CH, Chen M, Wayne Chang WS, Chen JY.** 2010. Epstein-Barr virus DNase (BGLF5) induces genomic instability in human epithelial cells. Nucleic Acids Res **38:**1932-1949.

38. **Xiao Y, Chen J, Liao Q, Wu Y, Peng C, Chen X.** 2013. Lytic infection of Kaposi's sarcoma-associated herpesvirus induces DNA double-strand breaks and impairs non-homologous end joining. J Gen Virol **94:**1870-1875.
39. **Nikitin PA, Luftig MA.** 2011. At a crossroads: human DNA tumor viruses and the host DNA damage response. Future Virol **6:**813-830.
40. **Nikitin PA, Luftig MA.** 2012. The DNA damage response in viral-induced cellular transformation. Br J Cancer **106:**429-435.
41. **Keles H, Fidan AF, Cigerci IH, Kucukkurt I, Karadas E, Dundar Y.** 2010. Increased DNA damage and oxidative stress in chickens with natural Marek's disease. Vet Immunol Immunopathol **133:**51-58.
42. **Dorange F, El Mehdaoui S, Pichon C, Coursaget P, Vautherot JF.** 2000. Marek's disease virus (MDV) homologues of herpes simplex virus type 1 UL49 (VP22) and UL48 (VP16) genes: high-level expression and characterization of MDV-1 VP22 and VP16. J Gen Virol **81:**2219-2230.
43. **Denesvre C, Remy S, Trapp-Fragnet L, Smith LP, Georgeault S, Vautherot JF, Nair V.** 2015. Marek's disease virus undergoes complete morphogenesis after reactivation in T-lymphoblastoid cell line transformed by recombinant fluorescent marker virus. J Gen Virol doi:10.1099/jgv.0.000354**:**DOI: 10.1099/jgv.1090.000354.
44. **Pratt WD, Morgan RW, Schat KA.** 1992. Characterization of reticuloendotheliosis virus-transformed avian T-lymphoblastoid cell lines infected with Marek's disease virus. J Virol **66:**7239-7244.
45. **Blondeau C, Marc D, Courvoisier K, Vautherot JF, Denesvre C.** 2008. Functional homologies between avian and human alphaherpesvirus VP22 proteins in cell-to-cell spreading as revealed by a new cis-complementation assay. J Virol **82:**9278-9282.
46. **Jarosinski KW, Margulis NG, Kamil JP, Spatz SJ, Nair VK, Osterrieder N.** 2007. Horizontal transmission of Marek's disease virus requires US2, the UL13 protein kinase, and gC. J Virol **81:**10575-10587.
47. **Arumugaswami V, Kumar PM, Konjufca V, Dienglewicz RL, Reddy SM, Parcells MS.** 2009. Latency of Marek's disease virus (MDV) in a reticuloendotheliosis virus-transformed T-cell line. II: expression of the latent MDV genome. Avian Dis **53:**156-165.
48. **Jarosinski KW, Yunis R, O'Connell PH, Markowski-Grimsrud CJ, Schat KA.** 2002. Influence of genetic resistance of the chicken and virulence of Marek's disease virus (MDV) on nitric oxide responses after MDV infection. Avian Dis **46:**636-649.
49. **Lebailly P, Devaux A, Pottier D, De Meo M, Andre V, Baldi I, Severin F, Bernaud J, Durand B, Henry-Amar M, Gauduchon P.** 2003. Urine mutagenicity and lymphocyte DNA damage in fruit growers occupationally exposed to the fungicide captan. Occup Environ Med **60:**910-917.
50. **Ding AH, Nathan CF, Stuehr DJ.** 1988. Release of reactive nitrogen intermediates and reactive oxygen intermediates from mouse peritoneal macrophages. Comparison of activating cytokines and evidence for independent production. J Immunol **141:**2407-2412.
51. **Walker JV, Nitiss JL.** 2002. DNA topoisomerase II as a target for cancer chemotherapy. Cancer Invest **20:**570-589.
52. **Barzilai A, Yamamoto K.** 2004. DNA damage responses to oxidative stress. DNA Repair (Amst) **3:**1109-1115.
53. **Phoa N, Epe B.** 2002. Influence of nitric oxide on the generation and repair of oxidative DNA damage in mammalian cells. Carcinogenesis **23:**469-475.
54. **Calnek BW, Schat KA, Ross LJ, Chen CL.** 1984. Further characterization of Marek's disease virus-infected lymphocytes. II. In vitro infection. Int J Cancer **33:**399-406.
55. **Shek WR, Calnek BW, Schat KA, Chen CH.** 1983. Characterization of Marek's disease virus-infected lymphocytes: discrimination between cytolytically and latently infected cells. J Natl Cancer Inst **70:**485-491.
56. **Palmai-Pallag T, Bachrati CZ.** 2014. Inflammation-induced DNA damage and damage-induced inflammation: a vicious cycle. Microbes Infect **16:**822-832.

57. **Jaiswal M, LaRusso NF, Burgart LJ, Gores GJ.** 2000. Inflammatory cytokines induce DNA damage and inhibit DNA repair in cholangiocarcinoma cells by a nitric oxide-dependent mechanism. Cancer Res **60:**184-190.
58. **Jaiswal H, Lindqvist A.** 2015. Bystander communication and cell cycle decisions after DNA damage. Front Genet **6:**63.
59. **Elliott G, O'Hare P.** 1997. Intercellular trafficking and protein delivery by a herpesvirus structural protein. Cell **88:**223-233.
60. **Wu F, Long J, Wang S, Xing J, Li M, Zheng C.** 2012. Live cell imaging fails to support viral-protein-mediated intercellular trafficking. Arch Virol **157:**1383-1386.
61. **Xue X, Huang J, Wang H.** 2014. The study of the intercellular trafficking of the fusion proteins of herpes simplex virus protein VP22. PLoS One **9:**e100840.
62. **Djeraba A, Bernardet N, Dambrine G, Quere P.** 2000. Nitric oxide inhibits Marek's disease virus replication but is not the single decisive factor in interferon-gamma-mediated viral inhibition. Virology **277:**58-65.
63. **Xing Z, Schat KA.** 2000. Inhibitory effects of nitric oxide and gamma interferon on in vitro and in vivo replication of Marek's disease virus. J Virol **74:**3605-3612.
64. **Karanjawala ZE, Murphy N, Hinton DR, Hsieh CL, Lieber MR.** 2002. Oxygen metabolism causes chromosome breaks and is associated with the neuronal apoptosis observed in DNA double-strand break repair mutants. Curr Biol **12:**397-402.
65. **Weitzman MD, Lilley CE, Chaurushiya MS.** 2010. Genomes in conflict: maintaining genome integrity during virus infection. Annu Rev Microbiol **64:**61-81.
66. **Guo Z, Deshpande R, Paull TT.** 2010. ATM activation in the presence of oxidative stress. Cell Cycle **9:**4805-4811.
67. **Guo Z, Kozlov S, Lavin MF, Person MD, Paull TT.** 2010. ATM activation by oxidative stress. Science **330:**517-521.
68. **E X, Pickering MT, Debatis M, Castillo J, Lagadinos A, Wang S, Lu S, Kowalik TF.** 2011. An E2F1-mediated DNA damage response contributes to the replication of human cytomegalovirus. PLoS Pathog **7:**e1001342.
69. **Kudoh A, Fujita M, Zhang L, Shirata N, Daikoku T, Sugaya Y, Isomura H, Nishiyama Y, Tsurumi T.** 2005. Epstein-Barr virus lytic replication elicits ATM checkpoint signal transduction while providing an S-phase-like cellular environment. J Biol Chem **280:**8156-8163.
70. **Shirata N, Kudoh A, Daikoku T, Tatsumi Y, Fujita M, Kiyono T, Sugaya Y, Isomura H, Ishizaki K, Tsurumi T.** 2005. Activation of ataxia telangiectasia-mutated DNA damage checkpoint signal transduction elicited by herpes simplex virus infection. J Biol Chem **280:**30336-30341.
71. **Bohgaki T, Bohgaki M, Hakem R.** 2010. DNA double-strand break signaling and human disorders. Genome Integr **1:**15.
72. **Bill CA, Summers J.** 2004. Genomic DNA double-strand breaks are targets for hepadnaviral DNA integration. Proc Natl Acad Sci U S A **101:**11135-11140.
73. **Chen Y, Williams V, Filippova M, Filippov V, Duerksen-Hughes P.** 2014. Viral carcinogenesis: factors inducing DNA damage and virus integration. Cancers (Basel) **6:**2155-2186.

694 **FIGURE LEGENDS**

695 **Figure 1. Induction of DNA damage in MDV lytically infected cells.** CESCs were infected
696 with 10^4 pfu of recEGFPVP22. (A) DNA damage analysis in mock- or recEGFPVP22-
697 infected CESCs. At 4 dpi, EGFP-positive and -negative cells were sorted by flow cytometry
698 and DNA damage was analyzed from $2x10^5$ cells by alkaline comet assays. Two slides per
699 comet assays were prepared for each condition and analyzed using the CometScore software.
700 Results are presented as the mean of OTM score (± SD; ***p<0,001) and representative
701 images of comets are shown as photographs. (B) Frequency distribution of the comets with
702 respect to their OTM value. (C) Expression and localization of γH2AX in CESCs infected
703 with recEGFPVP22. At 4 dpi, mock- and recEGFPVP22-infected CESCs were subjected to
704 immunofluorescence using a mouse anti-γH2AX monoclonal antibody and an AlexaFluor
705 594-conjugated secondary antibody (red). Nuclei were stained with Hoechst 33342 (blue) and
706 infected cells expressing the EGFP-tagged VP22 were directly visualized by fluorescent
707 microscopy (green).

708 **Figure 2. DNA damage induction enhances MDV replication.** (A-D) CESCs were infected
709 with recEGFPVP22 and treated at 6 hpi with etoposide (ETP), Bleomycin, hydroxyurea (HU)
710 and H_2O_2 at the indicated concentrations or with DMSO or H_2O (as negative controls). (A-B)
711 At 24, 48, 72, and 96 hpi, DNA was extracted from cells treated with ETP and MDV
712 replication was assessed using qPCR. For each group, the number of MDV genome copies
713 (corresponding to ICP4 copies number) was normalized to 10^6 cells (estimated by the iNOS
714 copies number). (A) Representative growth curve from a total of 3 independent experiments.
715 Means of qPCR triplicates are indicated (± SD). (B) Fold change in MDV copies in ETP-
716 treated cells relative to DMSO-treated cells (**p<0.05). (C) Number of cells lytically infected
717 with MDV upon ETP treatment. The percentage of viable GFP positive infected cells was
718 determined at 96 hpi by FACS. Viable cells were detected using the viability dye eFluor-780.

719 Means are represented as bars (± SD; *p<0.05). (D) Effect of ETP on MDV plaques size.
720 Images of fluorescent MDV plaques were taken and plaque sizes measured at 48 hpi. Means
721 are presented as histograms (± SD; *p<0.05; ***p<0.001). (E) Impact of ETP induced DNA
722 damage on MDV replication in RECC-CU91 T-cells. (E) RECC-CU91 cells were infected
723 with RB-1B_TK-GFP and treated with 0.02 and 0.1 µM of ETP or with DMSO (as a negative
724 control). At 24, 48 and 72 hpi, MDV genome copy number was quantified by qPCR and data
725 shown as a fold change (± SD) relative to DMSO-treated cells.

726 **Figure 3. MDV replication induces production of ROS and NO.** CESCs were mock-
727 infected or infected with recEGFPVP22. (A) ROS accumulation in supernatant of mock- and
728 recEGFPVP22-infected cells. At 24, 48, 72, and 96 hpi, supernatants of mock- and
729 recEGFPVP22-infected cells were collected, and H_2O_2 accumulation was quantified using the
730 ROS-Glo™ kit (Promega). Results were normalized to RLU values obtained from mock-
731 infected cells and expressed as means (± SD). (B) NO production in supernatant of mock- and
732 recEGFPVP22-infected cells. At indicated time points, supernatants of mock- and
733 recEGFPVP22-infected cells were collected, and nitrite accumulation was quantified using
734 the Griess reaction. Absorbance values (at 540 nm) obtained from supernatant of infected
735 cells were reported to these from mock-infected cells and expressed as means (± SD). (C)
736 Expression of inducible nitric oxide synthase (iNOS) in MDV infected cells. Total mRNA
737 was isolated from mock- and MDV infected CESCs at the time point indicated and qRT-PCR
738 were performed with iNOS specific primers. Results were normalized to GAPDH expression
739 and expressed as mRNA fold change compared to expression of iNOS in mock-infected cells
740 (± SD).

741 **Figure 4. Induction of DNA damage in PBMCs of chickens infected with MDV.** Specific
742 pathogen free (SPF) susceptible white leghorn chicks (B13/B13 haplotype) were inoculated
743 intramuscularly with 1,000 pfu of the very virulent MDV strain vRB-1B. DNA damage onset

744 in PBMCs was assessed in 10 non-infected chickens (circles) and 13 birds infected with vRB-
745 1B (triangles). Blood was collected from all birds at indicated time points. (A) DNA damage
746 analysis in PBMCs isolated from mock- and vRB-1B infected chickens by alkaline comet
747 assays. Two slides per comet assays were prepared for each animal at each time point. A
748 minimum of 50 comets were observed and further analyzed on each replicate slide using the
749 CometScore software. Results are presented as dot plot, each dot representing an animal and
750 the mean of OTM for each group is indicated as a bar (***$p<0.001$). (B) Viral load estimated
751 after DNA extraction from whole blood and quantification of MDV genome copies using
752 qPCR. For each group, the number of ICP4 copies in the MDV genome was normalized to
753 10^6 copies of cellular genome estimated by the detection of iNOS copies. The medians copy
754 numbers are indicated as a bar. (C) Meq mRNA expression upon MDV infection. Total RNA
755 was extracted from PBMCs isolated from blood of birds infected with vRB-1B. Quantitative
756 RT-PCRs were performed in order to detect the mRNA expression of Meq. Gene expression
757 was normalized to GAPDH expression and fold changes are presented as box plot (Min/max).

758 **Figure 5. Role of VP22 and DNA damage in MDV-mediated oncogenicity in chickens.**
759 SPF white leghorn chicks were inoculated with 1,500 pfu of vRB-1B, vRB-1B EGFP22, or
760 vRB-1B 22EGFP. Blood was collected from all birds at indicated time points and PBMCs
761 were isolated. (A) DNA damage was quantified from $2x10^5$ PBMCs using the alkaline comet
762 assay. Results are presented as dot plots, each dot representing an animal. For each group, the
763 median of the OTM is indicated as a bar (***$p<0.001$) (B). MDV viral load was evaluated by
764 qPCR on DNA extracted from PBMCs. The number of MDV copies per 10^6 cells is presented
765 as a dot plot, each dot representing an animal. For each group, the median is indicated as a bar
766 (*$p<0.05$; **$p<0.005$).

767

768 **Figure 6. DNA damage during MDV reactivation**.

769 3867K cells undergoing MDV lytic replication were sorted by cytometry on the basis of the
770 expression of the UL47 gene tagged with EGFP. (A) DNA damage analysis in lytically
771 (GFP+) and latently (GFP-) infected cells. The alkaline comet assay was performed on EGFP-
772 positive and -negative sorted cells. Results are presented as the mean of OTM (± SD;
773 ***p<0.001) and representative comets images are shown below. (B) Frequency distribution
774 of the comets with respect to their OTM value. (C-E) Effect of DNA damaging
775 pharmacological agents on MDV reactivation. 3867K cells were treated with etoposide
776 (ETP), bleomycin, hydroxyurea (HU) or H_2O_2 at the indicated concentrations for 48 hours.
777 DMSO and H_2O were added to culture media as negative controls. (C) MDV replication was
778 evaluated by quantifying the mRNA expression of the immediate-early gene ICP4 by qRT-
779 PCR. ICP4 expression was normalized to the expression of GAPDH and results are presented
780 as means (± SD; **p<0.005). (D-E) Number of MDV reactivated 3867K cells. The
781 percentage of GFP positive cells (expressing the EGFP-tagged UL47 protein) was determined
782 48 h post-treatment by cytometry specifically in viable cells labeled using the viability dye
783 eFluor-780. Means are represented as bars (± SD; *p<0.05). Results are representative of 3
784 independent experiments realized in triplicates.

Target		Sequences	Accession Number
ICP4	For	5'TTTCTAGCAAGGAGCGACGC3'	NC_002229.3
	Rev	5'CTGACTTGCGCTTACGGGAA3'	
Meq	For	5'GTCCCCCCTCGATCTTTCTC3'	AY571783.1
	Rev	5'CGTCTGCTTCCTGCGTCTTC3'	
iNOS	For	5'TACTGCGTGTCCTTTCAACG3'	U46504
	Rev	5'CCCATTCTTCTTCCAACCTC3'	
GAPDH	For	5'TGATGATATCAAGAGGGTAGTGAAG3'	K01458
	Rev	5'TCCTTGGATGCCATGTGGACCAT3'	

785 **Table 1. List of primer pairs used for (q)RT-PCR**

786

Treatment	**Concentration (µM)**	**Mean ICP4/10^6 iNOS copies**
H_2O		$(1.46\pm0,22)x10^8$
Bleomycin	0.125	$(1.33\pm0,05)x10^8$
	0.25	$(2.25\pm0,04)x10^8$
	0.5	$(2.16\pm0,14)x10^8$
	1	$(2.47\pm0,33)x10^8$
Hydroxyurea	10	$(2.55\pm0,03)x10^8$
	25	$(2.6\pm0,005)x10^8$
	50	$(1.76\pm0,03)x10^8$
	75	$(1.83\pm0,25)x10^8$
H_2O_2	12.5	$(1.91\pm0,009)x10^8$
	25	$(1.6\pm0,03)x10^8$
	50	$(1.38\pm0,05)x10^8$
	100	$(2.12\pm0,23)x10^8$

787 **Table 2. Effect of DNA damage inducers on MDV replication in CESCs**

788

Figure 1

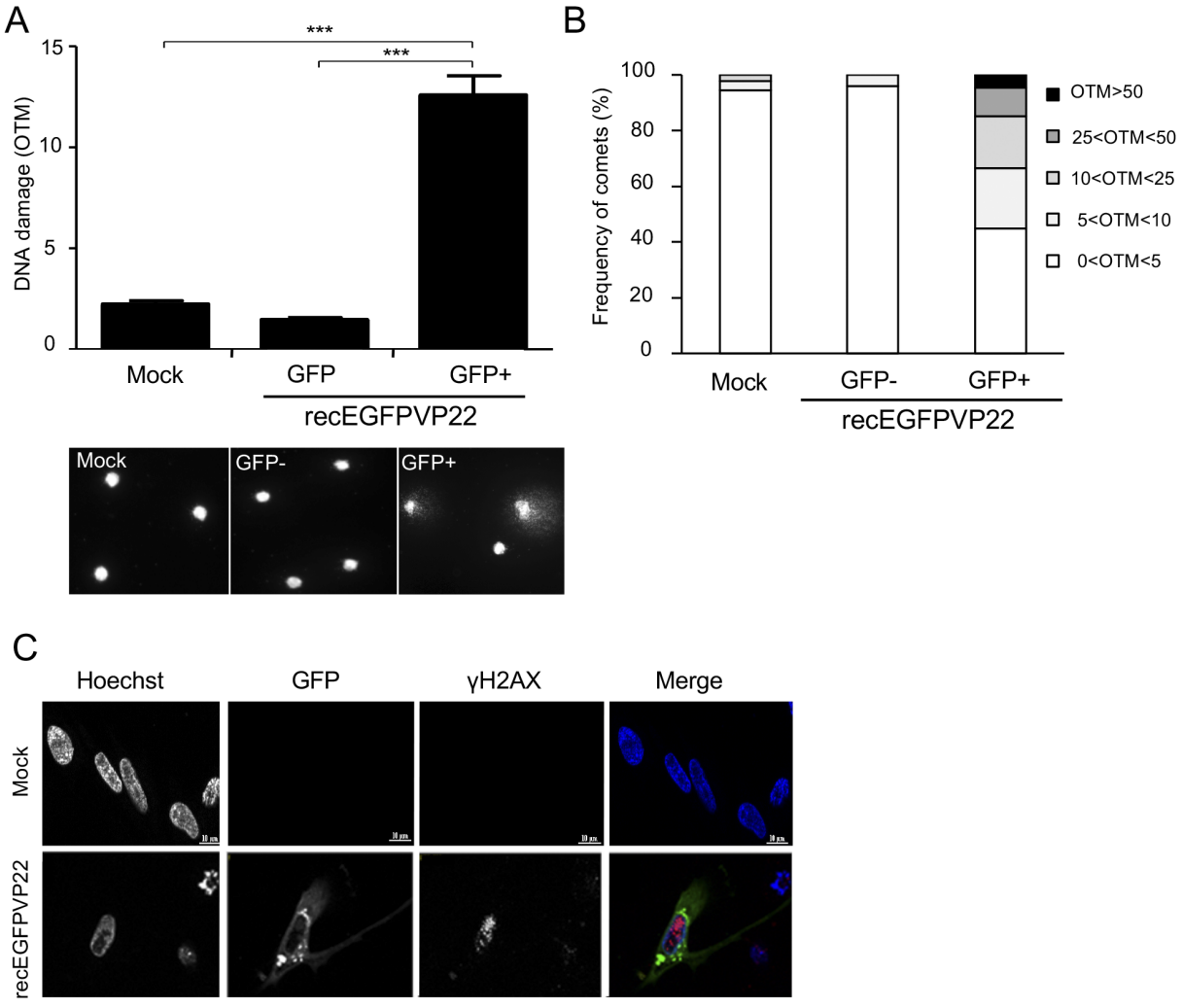

Figure 1. Induction of DNA damage in MDV lytically infected cells. CESCs were infected with 10^4 pfu of recEGFPVP22. (A) DNA damage analysis in mock- or recEGFPVP22-infected CESCs. At 4 dpi, EGFP-positive and -negative cells were sorted by flow cytometry and DNA damage was analyzed from $2x10^5$ cells by alkaline comet assays. Two slides per comet assays were prepared for each condition and analyzed using the CometScore software. Results are presented as the mean of OTM score (± SD; ***p<0,001) and representative images of comets are shown as photographs. (B) Frequency distribution of the comets with respect to their OTM value. (C) Expression and localization of γH2AX in CESCs infected with recEGFPVP22. At 4 dpi, mock- and recEGFPVP22-infected CESCs were subjected to immunofluorescence using a mouse anti-γH2AX monoclonal antibody and an AlexaFluor 594-conjugated secondary antibody (red). Nuclei were stained with Hoechst 33342 (blue) and infected cells expressing the EGFP-tagged VP22 were directly visualized by fluorescent microscopy (green).

Figure 2

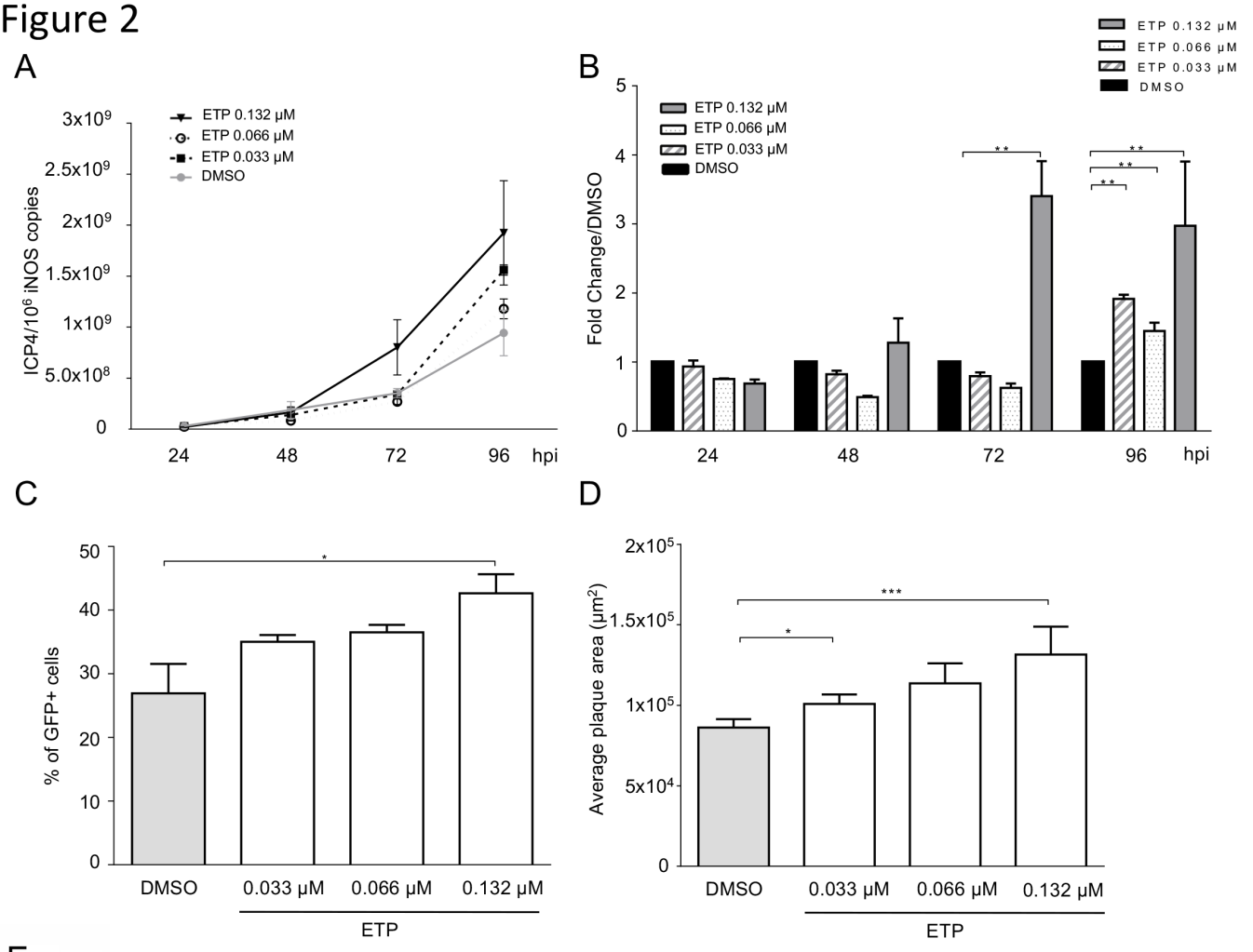

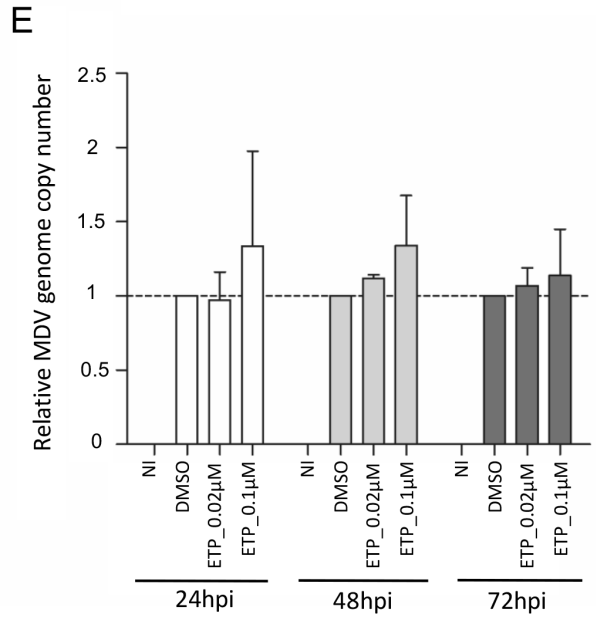

Figure 2. DNA damage induction enhances MDV replication. (A-D) CESCs were infected with recEGFPVP22 and treated at 6 hpi with etoposide (ETP), Bleomycin, hydroxyurea (HU) and H2O2 at the indicated concentrations or with DMSO or H2O (as negative controls). (A-B) At 24, 48, 72, and 96 hpi, DNA was extracted from cells treated with ETP and MDV replication was assessed using qPCR. For each group, the number of MDV genome copies (corresponding to ICP4 copies number) was normalized to 10^6 cells (estimated by the iNOS copies number). (A) Representative growth curve from a total of 3 independent experiments. Means of qPCR triplicates are indicated (± SD). (B) Fold change in MDV copies in ETP-treated cells relative to DMSO-treated cells (**p<0.05). (C) Number of cells lytically infected with MDV upon ETP treatment. The percentage of viable GFP positive infected cells was determined at 96 hpi by FACS. Viable cells were detected using the viability dye eFluor-780. Means are represented as bars (± SD; *p<0.05). (D) Effect of ETP on MDV plaques size. Images of fluorescent MDV plaques were taken and plaque sizes measured at 48 hpi. Means are presented as histograms (± SD; *p<0.05; ***p<0.001). (E) Impact of ETP induced DNA damage on MDV replication in RECC-CU91 T-cells. (E) RECC-CU91 cells were infected with RB-1B TK-GFP and treated with 0.02 and 0.1 µM of ETP or with DMSO (as a negative control). At 24, 48 and 72 hpi, MDV genome copy number was quantified by qPCR and data shown as a fold change (± SD) relative to DMSO-treated cells.

Figure 3

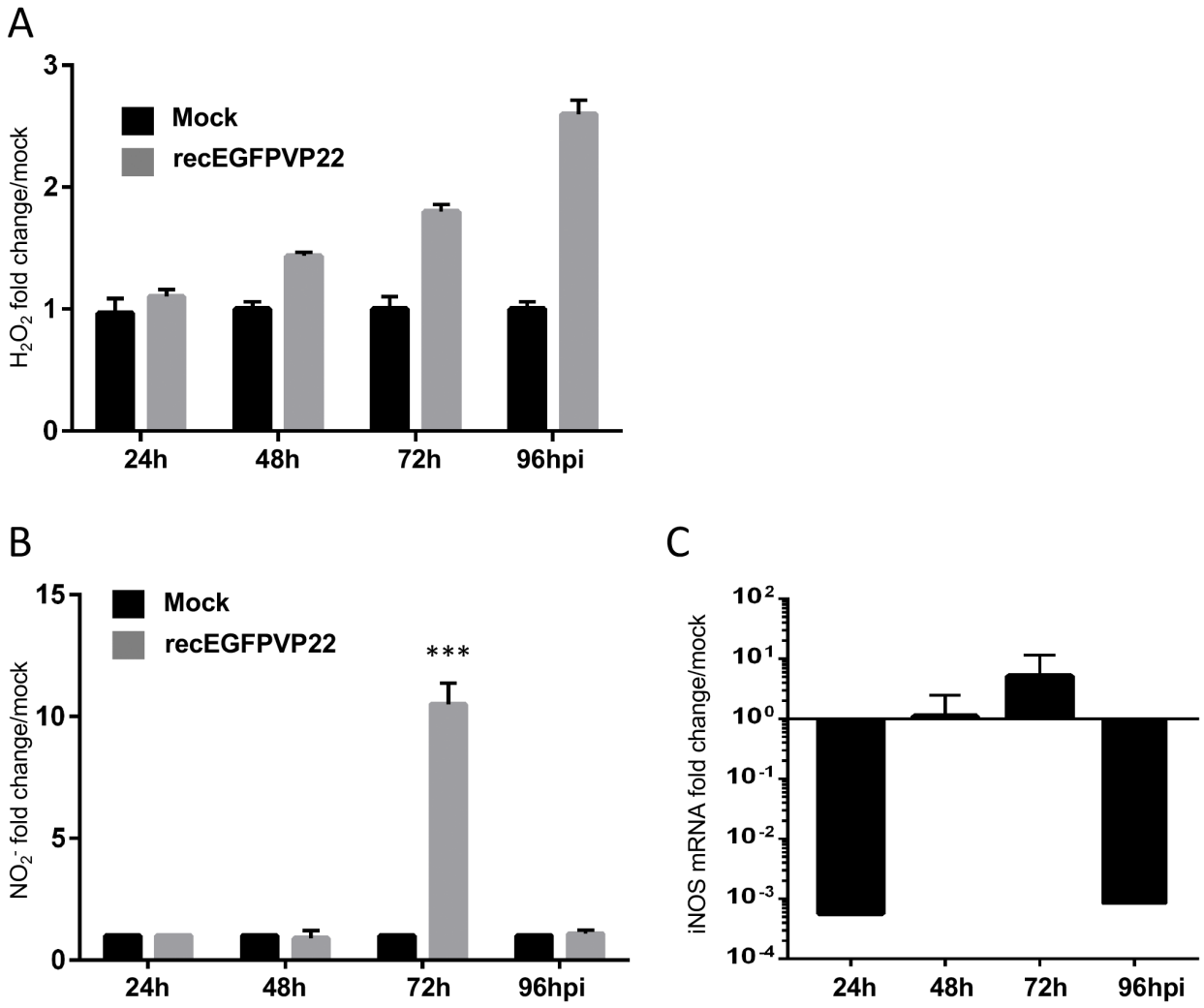

Figure 3. MDV replication induces production of ROS and NO. CESCs were mock-infected or infected with recEGFPVP22. (A) ROS accumulation in supernatant of mock- and recEGFPVP22-infected cells. At 24, 48, 72, and 96 hpi, supernatants of mock- and recEGFPVP22-infected cells were collected, and H2O2 accumulation was quantified using the ROS-GloTM kit (Promega). Results were normalized to RLU values obtained from mock-infected cells and expressed as means (± SD). (B) NO production in supernatant of mock- and recEGFPVP22-infected cells. At indicated time points, supernatants of mock- and recEGFPVP22-infected cells were collected, and nitrite accumulation was quantified using the Griess reaction. Absorbance values (at 540 nm) obtained from supernatant of infected cells were reported to these from mock-infected cells and expressed as means (± SD). (C) Expression of inducible nitric oxide synthase (iNOS) in MDV infected cells. Total mRNA was isolated from mock- and MDV infected CESCs at the time point indicated and qRT-PCR were performed with iNOS specific primers. Results were normalized to GAPDH expression and expressed as mRNA fold change compared to expression of iNOS in mock-infected cells (± SD).

Figure 4

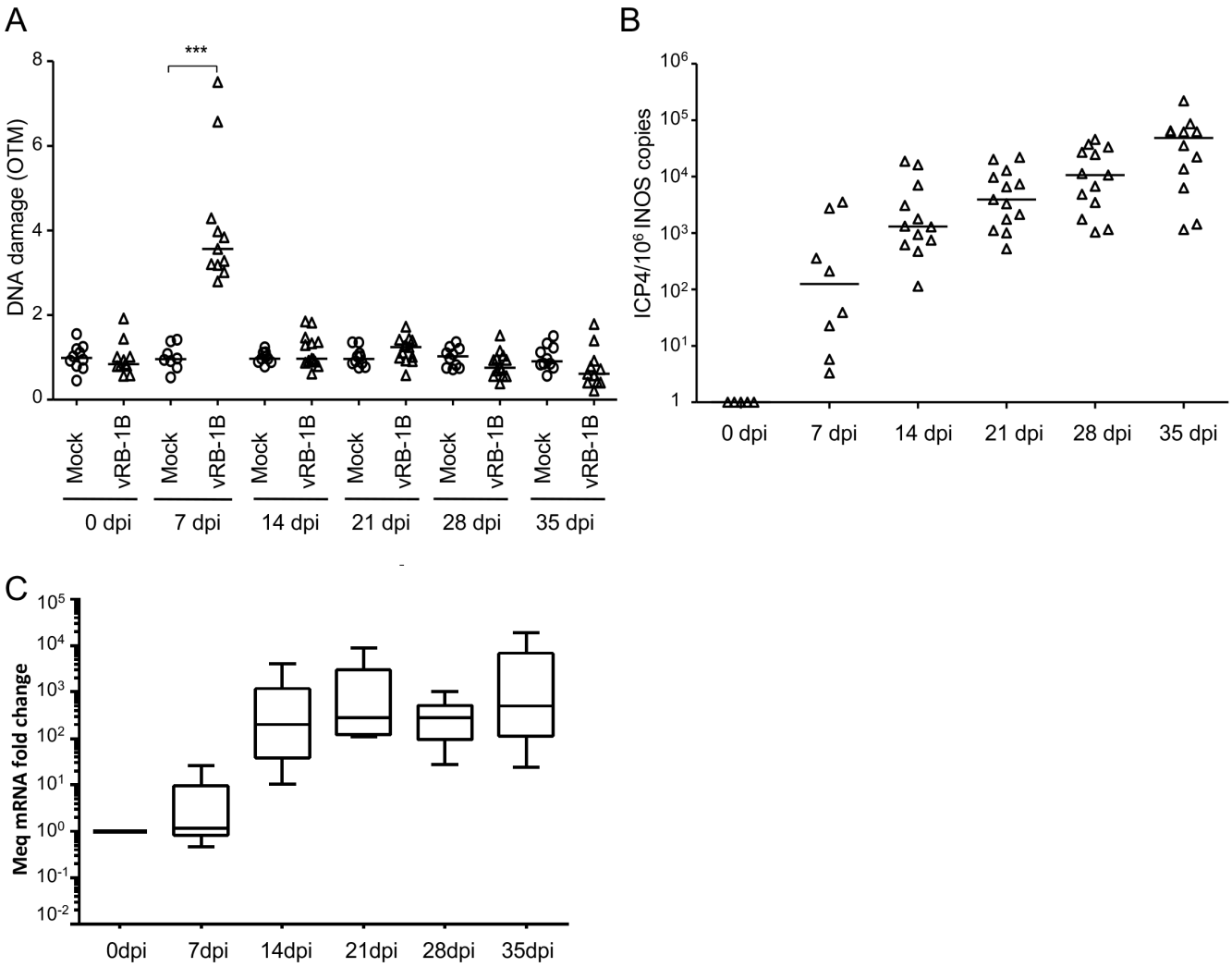

Figure 4. Induction of DNA damage in PBMCs of chickens infected with MDV. Specific pathogen free (SPF) susceptible white leghorn chicks (B13/B13 haplotype) were inoculated intramuscularly with 1,000 pfu of the very virulent MDV strain vRB-1B. DNA damage onset in PBMCs was assessed in 10 non-infected chickens (circles) and 13 birds infected with vRB-1B (triangles). Blood was collected from all birds at indicated time points. (A) DNA damage analysis in PBMCs isolated from mock- and vRB-1B infected chickens by alkaline comet assays. Two slides per comet assays were prepared for each animal at each time point. A minimum of 50 comets were observed and further analyzed on each replicate slide using the CometScore software. Results are presented as dot plot, each dot representing an animal and the mean of OTM for each group is indicated as a bar (***$p<0.001$). (B) Viral load estimated after DNA extraction from whole blood and quantification of MDV genome copies using qPCR. For each group, the number of ICP4 copies in the MDV genome was normalized to 10^6 copies of cellular genome estimated by the detection of iNOS copies. The medians copy numbers are indicated as a bar. (C) Meq mRNA expression upon MDV infection. Total RNA was extracted from PBMCs isolated from blood of birds infected with vRB-1B. Quantitative RT-PCRs were performed in order to detect the mRNA expression Meq. Gene expression was normalized to GAPDH expression and fold changes are presented as box plot (Min/max).

Figure 5

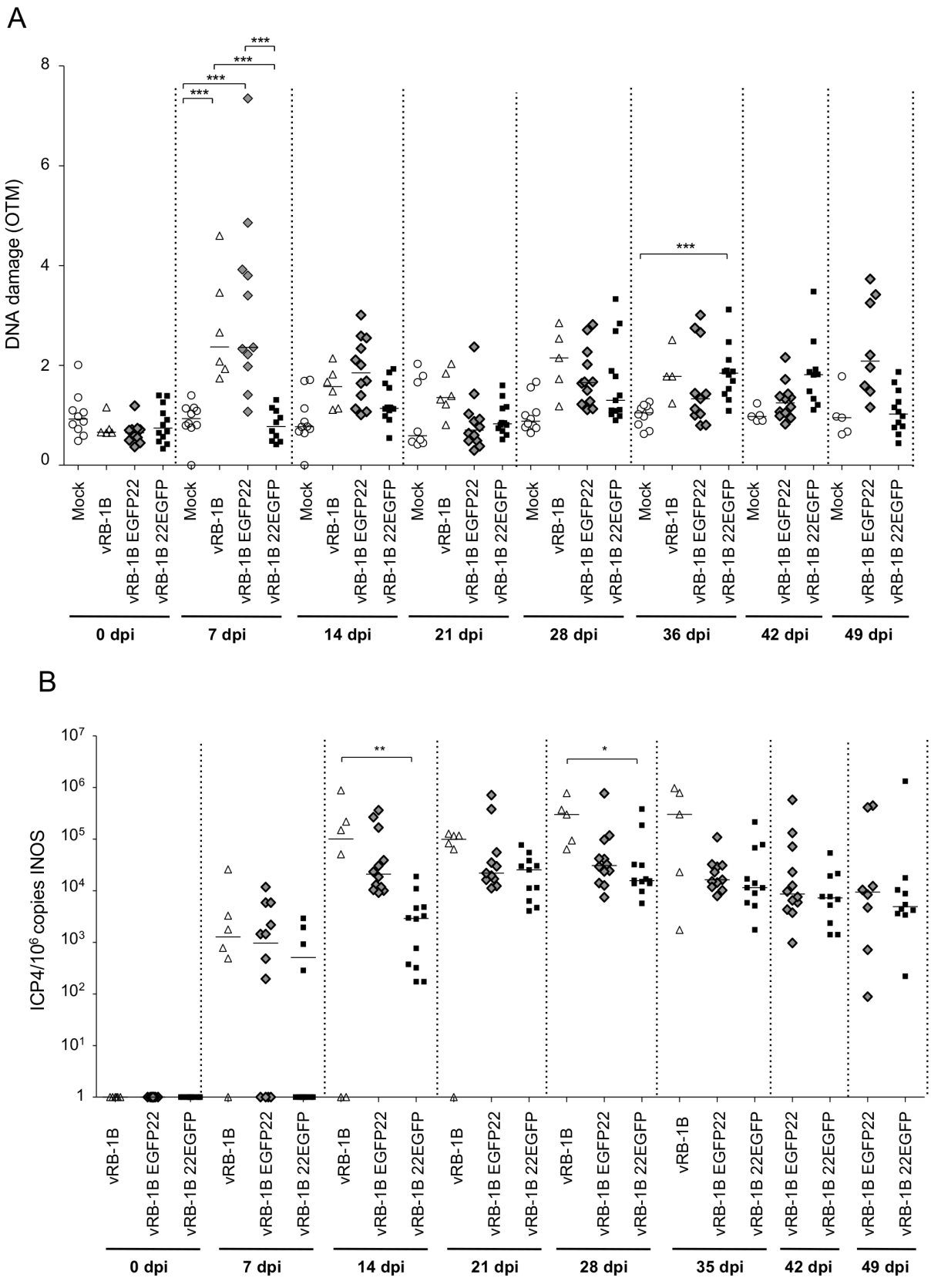

Figure 6

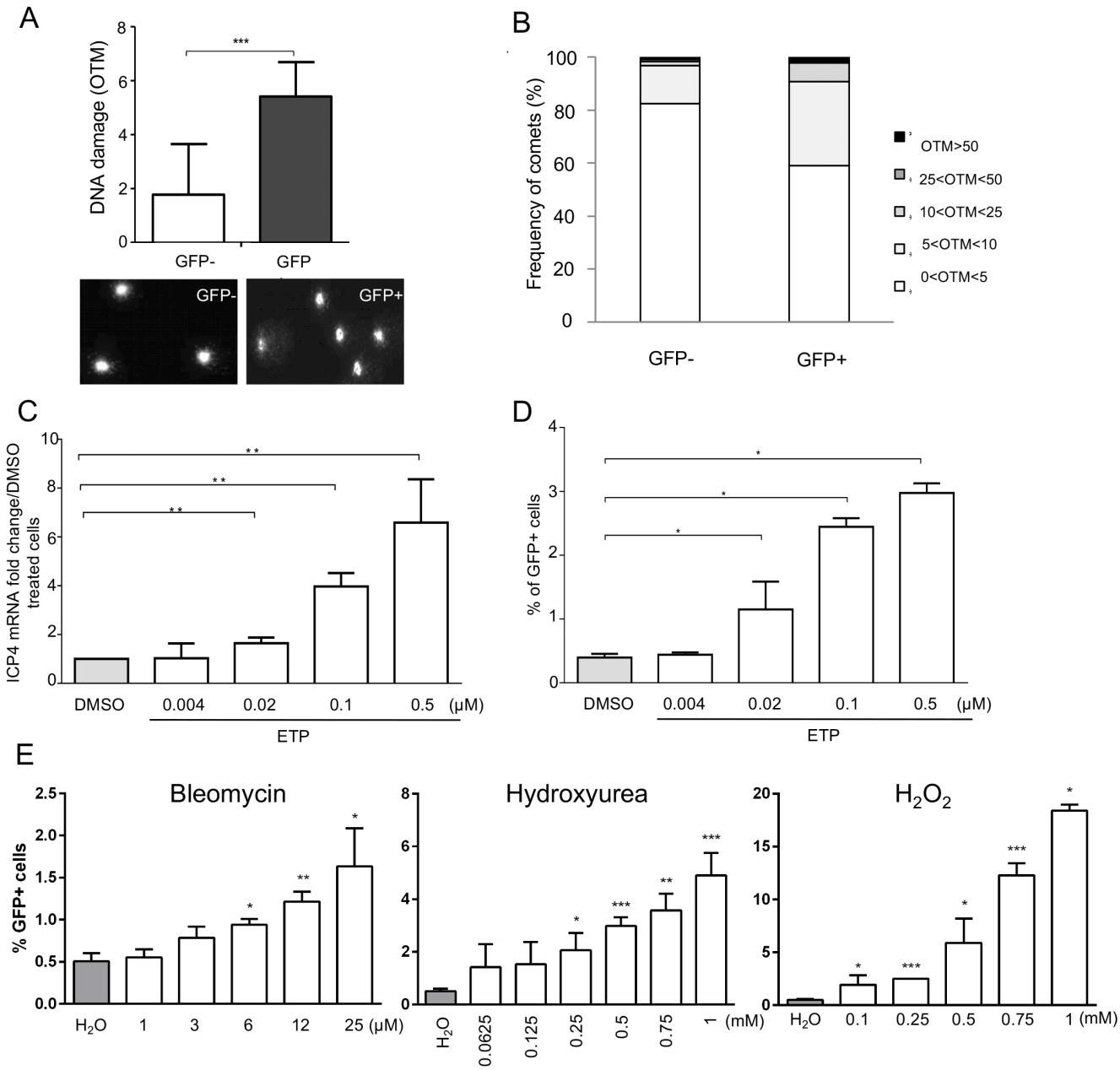

Figure 6. DNA damage during MDV reactivation. 3867(K) cells undergoing MDV lytic replication were sorted by cytometry on the basis of the expression of the UL47 gene tagged with EGFP. (A) DNA damage analysis in lytically (GFP+) and latently (GFP-) infected cells. The alkaline comet assay was performed on EGFP-positive and -negative sorted cells. Results are presented as the mean of OTM (± SD; ***p<0.001) and representative comets images are shown below. (B) Frequency distribution of the comets with respect to their OTM value. (C-E) Effect of DNA damaging pharmacological agents on MDV reactivation. 3867(K) cells were treated with etoposide (ETP), bleomycin, hydroxyurea (HU) or H2O2 at the indicated concentrations for 48 hours. DMSO and H2O were added to culture media as negative controls. (C) MDV replication was evaluated by quantifying the mRNA expression of the immediate-early gene ICP4 by qRT-PCR. ICP4 expression was normalized to the expression of GAPDH and results are presented as means (± SD; **p<0.005). (D-E) Number of MDV reactivated 3867(K) cells. The percentage of GFP positive cells (expressing the EGFP-tagged UL47 protein) was determined 48 h post-treatment by cytometry specifically in viable cells labeled using the viability dye eFluor-780. Means are represented as bars (± SD; *p<0.05). Results are representative of 3 independent experiments realized in triplicates.